A simulation investigation into the effects of sea level rise on tidal propagation in fjords.

Campbell Glass

glassctm@uw.edu

University of Washington, School of Oceanography, Seattle, Washington 98195

Under the advisement of Mitsuhiro Kawase and Miles Logsdon

June 1 2015

Acknowledgments

Many thanks to Mitsuhiro Kawase, without whom my model and mind would have been much less stable. Thanks as well to Miles Logsdon, for being willing to philosophize on short notice. Special thanks also to Arthur Nowell for providing precious understanding, empathy, and feedback. Further thanks go to the small boat crew and their good captain Dave, for being the best possible companions on bracing adventures at sea. Finally I'd like to thank all of the students and faculty of the senior thesis class for being a fantastic and helpful bunch.

0. Abstract

Sea level rise projected to occur in the 21st century will undoubtedly influence coastal marine environments, although the exact effects are unknown. A two-dimensional numerical simulation model of tidal circulation is used to investigate the impacts of sea level rise on a fjord in terms of the distribution of kinetic energy throughout said fjord. Sea level is altered over a number of separate simulations, and the kinetic energy output is examined as a measure of how fluid flow will change as a result of sea level variation. Kinetic energy was found to change most in shallow sill areas, whereas other areas such as the deeper body of the fjord and the shallow intertidal zones showed very little change in kinetic energy. Furthermore, some protruding headland-like coastal features were found to experience significant shifts in the amount of kinetic energy that they experience, which may cause increased erosion on their flanks and/or increased deposition on their heads. These changes in sediment transport could result in significant changes to overall circulation in the fjord should the shape of the fjord mouth change. These results could be generalized to infer what may happen in other fjord systems in the event of sea level rise, providing insight into how fjord environments and their inhabitants may be impacted by sea level rise and allowing for more effective preparation for the future.

1. Introduction

With further progression into the Anthropocene, the effects of human emissions will continue to influence the environment. One important component will be sea level rise, although the details of its many repercussions remain uncertain. Studying previous and future

effects of sea level rise on marine environments allows for preparation for and mitigation of any hazards that may arise. Past sea level change in the Pacific Northwest has occurred since the Last Glacial Maximum, changing regional sea levels by anywhere from -200 m to + 150 m (Shugar et al., 2014). Although the specific amount of future sea level rise we can expect is unknown, various models estimate an increase of 0.5 to 2.0 m by the year 2100, with further increase anticipated beyond that time (Church et al., 2013). In order to examine the effects that this sea level rise will have on fjords, a computational model of tidal circulation was used to simulate tides at the Nootka Sound fjord in British Columbia, Canada. This specific example of a fjord was used to make generalizations about the expected effects of sea level rise on fjords in general. While this approach required many considerations to ensure accuracy and applicability (Holleman and Stacey, 2014; Salehipour et al., 2013), it has previously been used to successfully investigate the tidal response to sea level rise in other areas (Pelling and Mattias Green, 2014). Investigating the effects that sea level rise may have on these coastal areas allows for more effective preparation for the future.

One important factor in marine environments is physical stress, which appears in many forms. Arguably the most important of these is the stress resulting from fluid flow through an ecosystem. This flow has many effects, from sediment transport to advection of nutrients to direct interactions with organisms. Consequently, changes in the location, direction, and strength of flow could have drastic impacts on the marine environment. This study investigates how the magnitude of kinetic energy throughout a fjord changes with sea level rise using a numerical simulation model of tidal circulation. These changes are expected to be dependent on the depth of the location in question due to the depth dependency present in the shallow-

water equations that will be used for modeling (Sadourny 1974). Deeper portions of the fjord are expected to see little change, while shallow areas such as river mouths and intertidal zones should see greater changes in the magnitude of kinetic energy that they experience. These shallow areas are also typically well-populated with marine life. Therefore, changes in kinetic energy may have a greater impact at these locations. Future investigation could determine specifically how these environments will be affected and respond to future sea level change.

The effect of sea level rise on fjords was investigated using a numerical simulation model of tidal circulation. Bathymetric data collected from existing online resources was used to create base surfaces for the model. Forcing and validation data were collected as part of the survey in order to ensure the accuracy of the model. Sea level was altered within the model, and the kinetic energy output was examined in order to ascertain how the physical climate of the region might change as a result of sea level variation. This examination provided insight into how fjord environments will be impacted by future sea level rise.

2. Methodology

2.1. Procedure

Investigation of how future sea level rise will impact estuarine tidal circulation was conducted using a two-dimensional ocean circulation model. This model was developed specifically for application in this study, and as such it was idealized and specialized for modeling tides in shallow fjords. The effects of sea level rise were examined by increasing sea level in simulations by amounts of 0 and 2.0 m. Following the increase in sea level, the simulations were run for a period of 10 days. Tides were allowed to propagate throughout the

model and the amount of kinetic energy present throughout the model domain was calculated. As the entirety of the model domain was sampled for analysis, the impacts of sea level rise on both shallow areas, such as the Gold River mouth, and deeper parts of the fjord, such as the main basin, could be investigated. This complete coverage allowed comparisons of the effects of sea level rise in different areas to be made in a thorough manner.

2.2. Bathymetry

The model domain, or area to be simulated, consists of Muchalat Inlet, a fjord composing part of Nootka Sound, British Columbia, Canada. Bathymetric data was obtained through the Canadian government web portal, *geogratis.ca*. This data for the inlet was initially presented at a resolution of 250m, but was spline interpolated down to the desired 100m resolution used in the model. The base surface can be seen in Figure 4

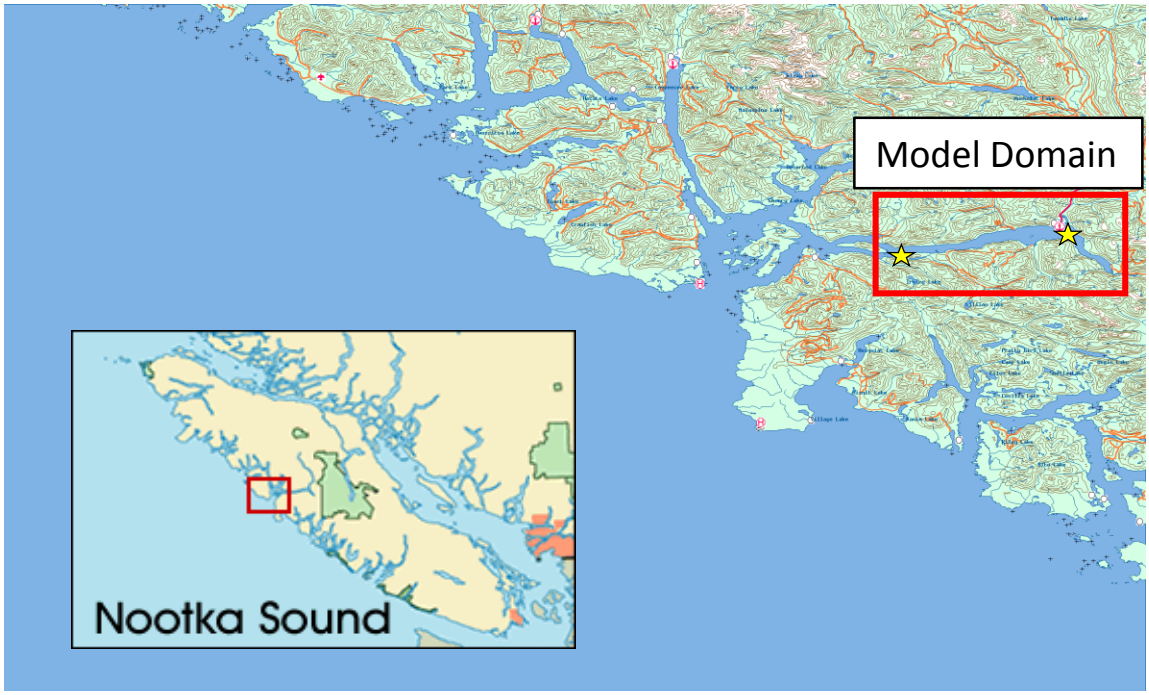

Figure 1: A map of the model domain and study site. Tidal gauges were placed at the starred locations. The western 'Gore Island' station provided forcing data, while the eastern 'Gold River' station provided validation data. Images obtained from http://static.flickr.com/27/40283487_df5793a67a_o.gif and http://www.canmaps.com/topomaps/nts250/toporama/092e.gif

2.3. Tides

Tidal data was collected at two locations at Muchalat Inlet, British Columbia, Canada using custom-built moorings, each bearing an 'Onset HOBO' 100-Foot Depth Water Level Data Logger. A rough schematic of the mooring is presented in Figure 2.

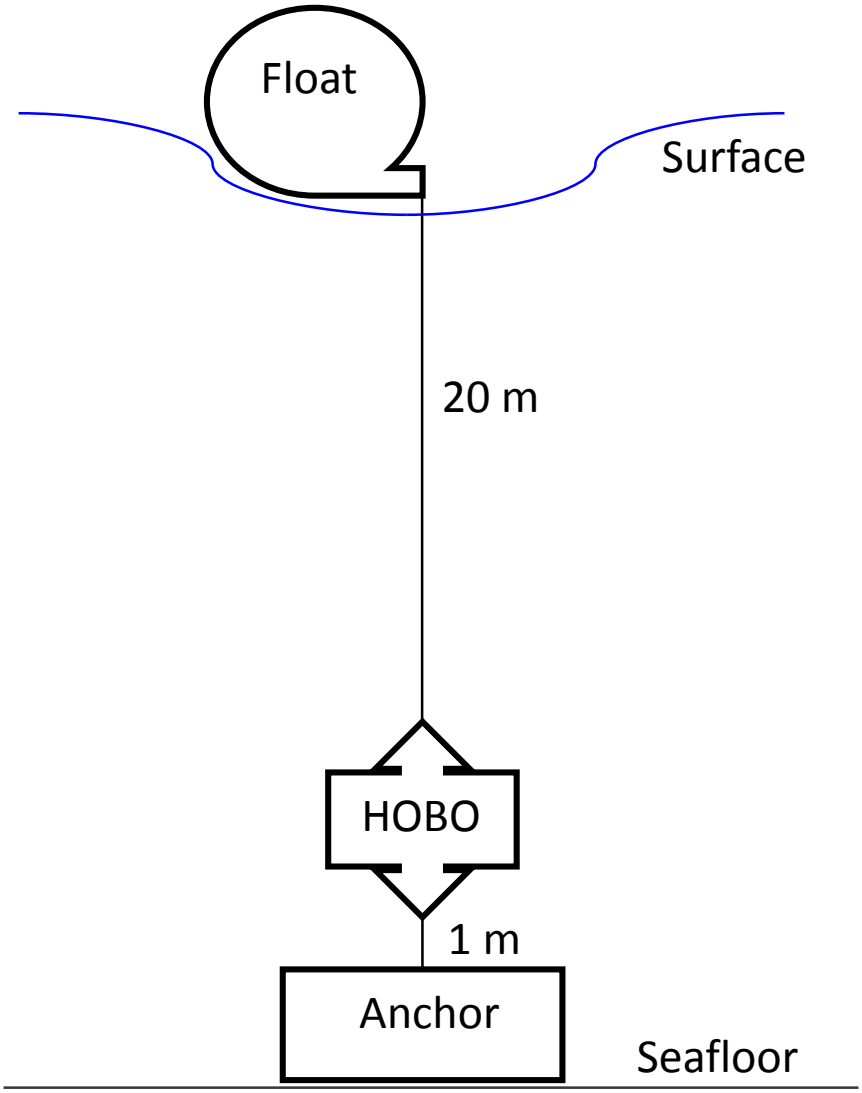

Figure 2: A design schematic of the moorings used to deploy tidal gauges at the study site. Each mooring consisted of an anchor connected by a rope to a float at the surface. The anchor sat on the seafloor with the data logger suspended approximately a meter above it. The float was primarily used for location and retrieval.

The collected tidal data was a vital component of the model. Water level data collected from the mooring at the mouth of Muchalat Inlet provided forcing data, while the second

mooring at the mouth of the Gold River provided validation data. These two data sets were required in order to ensure that the simulation was accurate and realistic.

Tidal harmonic analysis was performed on the collected data in order to calculate the tidal constituents. First, linear detrending of the tidal records was performed by fitting a linear function to the tidal record using the least-squares method. The calculated linear function was then subtracted from the tidal data. This served to remove most signals from non-tidal processes, such as seiche movement or wind setup, from the record. Following detrending, Fourier analysis was conducted to calculate the tidal constituents themselves (Schureman 1958).

2.4. Model equations

Calculations were performed using discretized versions of the two-dimensional nonlinear shallow-water wave equations (Sadourny 1974). These equations allow for both sea surface height and velocity in the x and y directions to be simulated, and are presented below. Note that u and v are velocities in the x and y directions respectively, t is time, B is the Bernoulli function, ζ is vorticity, f is the Coriolis force, g is gravity, H is mean sea level, and η is sea surface height. These first two equations are used to calculate acceleration in the x and y directions, respectively, which allow for future velocities to be predicted.

$$\frac{\partial u}{\partial t} = \frac{-\partial B}{\partial x} + v(\zeta + f) \quad [1]$$

$$\frac{\partial v}{\partial t} = \frac{-\partial B}{\partial y} - u(\zeta + f) \quad [2]$$

These next two equations define the Bernoulli function and vorticity. The Bernoulli function is proportional to the total amount of kinetic and potential energy present at a location. Vorticity is a measurement of how much rotational flow is present at a location, so a

higher vorticity indicates that more swirling is occurring.

$$B = g\eta + \frac{u^2+v^2}{2} \quad [3]$$

$$\zeta = \frac{\partial v}{\partial x} - \frac{\partial u}{\partial y} \quad [4]$$

This last equation is used to calculate the rate at which water is rising or falling at a location, which allows for future sea surface heights to be predicted.

$$\frac{\partial \eta}{\partial t} = \frac{-\partial}{\partial x}\big((H+\eta)u\big) - \frac{\partial}{\partial y}\big((H+\eta)v\big) \quad [5]$$

2.5. Friction

A quadratic bottom friction term was also included to ensure that accurate simulations are performed. This term, *F*, is of the following forms in the x and y direction.

$$F_x = \rho c_D \sqrt{u^2+v^2}u \quad [6]$$

$$F_y = \rho C_D \sqrt{u^2+v^2}v \quad [7]$$

Note that ρ is the density of the fluid, C_D is the drag coefficient, and u, v are velocity. These equations allow for the bottom friction experienced by water moving over the sea floor to be accounted for in the model. The standard dimensionless oceanic value of 0.003 was initially assumed for the drag coefficient (Durran 1998). While this value of the drag coefficient has precedence in modeling large scale processes, some papers have found more accurate results with values as high as 0.03 (Crean 1978, Kawase and Bang 2013). By performing multiple model runs with varying drag coefficient values and checking the output against validation data, the model could potentially be tuned to provide optimal results.

2.6. Grid

The model will be built on top of an Arakawa staggered c-grid (Arakawa 1977). An Arakawa staggered c-grid was chosen because it features four offset grids that allow for calculations of relevant properties at the centers, east-west and north-south boundaries, and corners of the model.

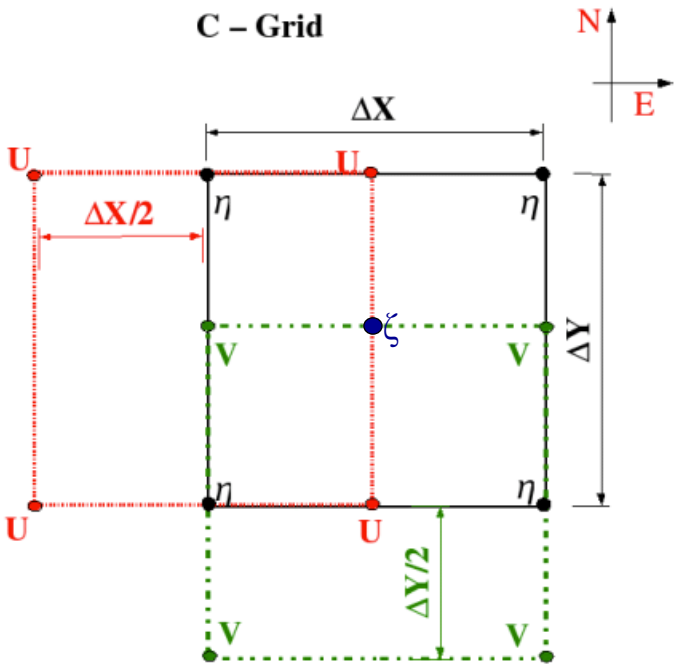

Figure 3: A single grid cell section of an Arakawa staggered c-grid. This grid configuration can be represented using four separate matrices: one for center values such as η, one for east-west boundary values such as u, one for north-south boundary values such as v, and one for corner values such as ζ. Image obtained from http://www.oceanographers.net/upload/vinu/layermodel/c-grid.gif

Coupled with bathymetric and water level data, these grid arrangements allow for full two-dimensional calculations to be performed using equations 1-7. When the model is set up with the proper tidal and bathymetric data, future sea surface height and water velocity values can be calculated.

2.7. Validation

Validation was conducted by calculating the error at tide gauge sites between the simulated time series sea surface height data and the recorded sea surface height data obtained by tidal gauges, as described in section 2.2. Both the Mean Absolute Error (MAE) and Root-Mean-Square Error (RMSE) were used to measure the error present in the model. The MAE was chosen because it measures the average magnitude of the difference between the simulated sea surface height data and the actual sea surface height data, which gives a quantitative measure of the simulation's accuracy. The MAE was calculated using the following equation:

$$MAE = \frac{1}{n}\sum_{i=1}^{n}|f_i - y_i| \quad [8]$$

In both the equations 8 and 9, f_i is the simulated sea surface height at time *i*, y_i is the actual sea surface height at time *i*, and *n* is the total number of measurements in each sea surface height time series.

The RMSE was chosen because it is similar to the MAE with one important difference: by squaring the error of individual data points, the errors become weighted by their own magnitudes. Thus, a data set with error concentrated in a few large outliers will have a higher RMSE than a data set with error spread out evenly throughout its elements. The RMSE was calculated using the following equation:

$$RMSE = \sqrt{\frac{1}{n}\sum_{i=1}^{n}(f_i - y_i)^2} \quad [9]$$

Using both of these error measures together gives a better picture of the overall model accuracy than either one would on its own.

Results

3.1. Bathymetry

Ranging from Gore Island in the west to the Gold River mouth in the east, the model domain consists of an area of roughly 100 km^2, measuring 5 km from North to South and 20 km from East to West. Below is a bathymetric map of the example fjord produced by interpolating data obtained through an online Canadian government data portal, *geogratis.ca*, to a 25 m resolution. The resulting surface is displayed below.

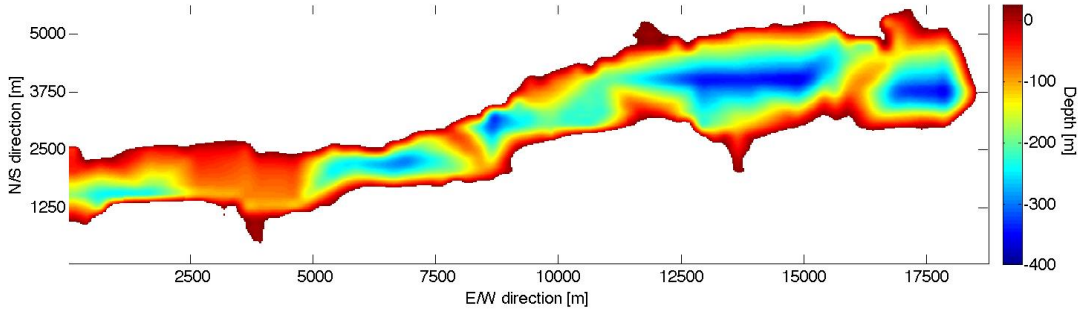

Figure 4: A bathymetric map of Muchalat Inlet. Note the long shallow sill between 2500 and 5000m along the channel. Also note the intermediate sill-pool pattern present in this data.

3.2. Tides

The following tidal constituents were calculated by detrending the tidal record and then applying Fourier analysis to calculate the magnitude of the following five tidal constituents: M_2, S_2, N_2, O_1, and K_1. Together, they account the majority of the observed tidal signal, as seen above, and combine to give a fairly accurate prediction of the tides at the study area.

A significant linear trend was observed in the forcing Gore Island station tidal data, on the order of +0.4m over the week (Figure 5). Correcting for the observed linear trend allowed computation of the M2, S2, N2, O1, and K1 tidal constituents (Table 1). These constituents were used to predict the tidal signal (Figure 6).

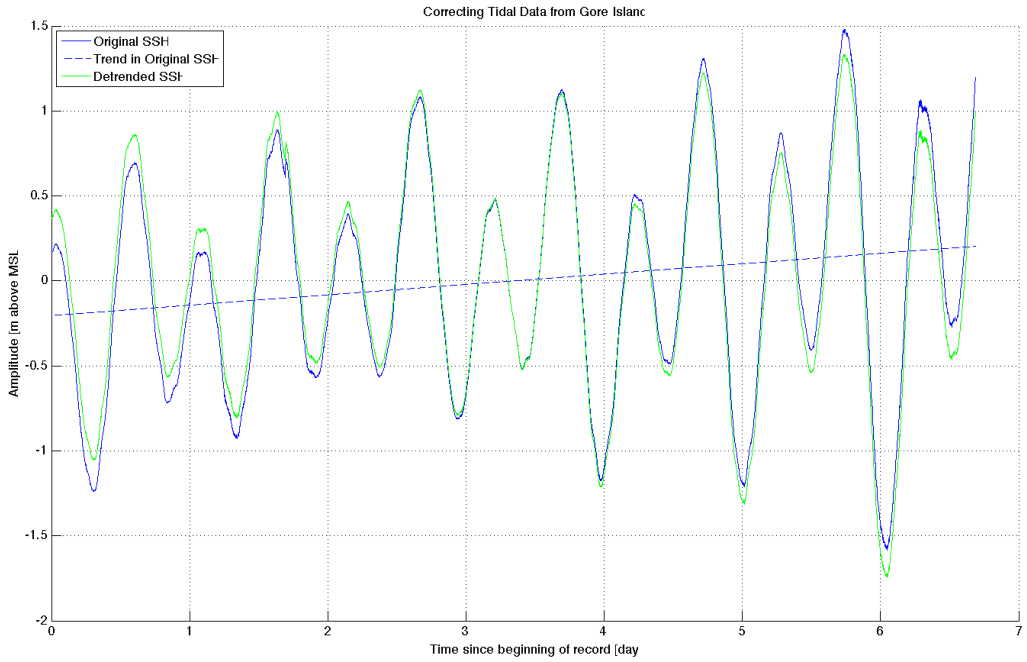

Figure 5: Raw observed Gore Island tidal data in green, with linear trend in dashed blue. Detrended tidal data shown in solid blue.

Gore Island Tidal Constituents

Constituent	Period [hr]	Amplitude [m]	Phase [radians]
M2	12.4206	0.9431	0.7537
S2	12	0.2359	-1.8826
N2	12.6583	0.0876	-2.7105
K1	23.9344	0.5444	-2.1500
O1	25.8193	0.2133	0.1248

Table 1: Major five tidal constituents present at the forcing Gore Island station.

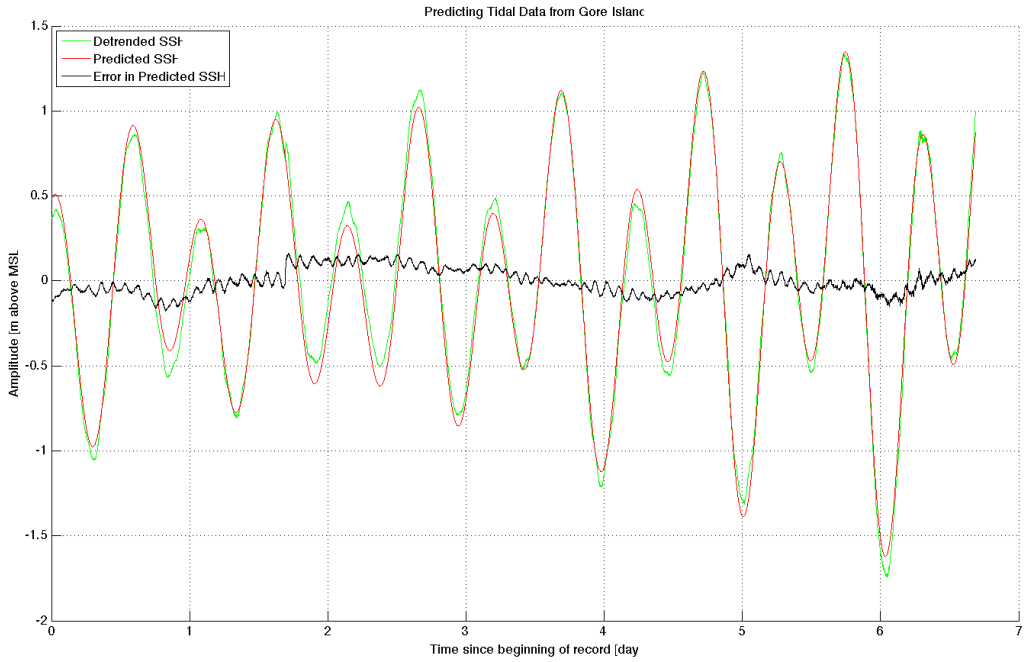

Figure 6: The predicted Gore Island tide in red compared to the observed data minus the linear trend in green. The difference between the two is shown in black.

A significant linear trend was observed in the forcing Gold River station tidal data, on the order of +0.3m over the week (Figure 7). Correcting for the observed linear trend allowed computation of the M2, S2, N2, O1, and K1 tidal constituents (Table 1). These constituents were used to predict the tidal signal (Figure 8).

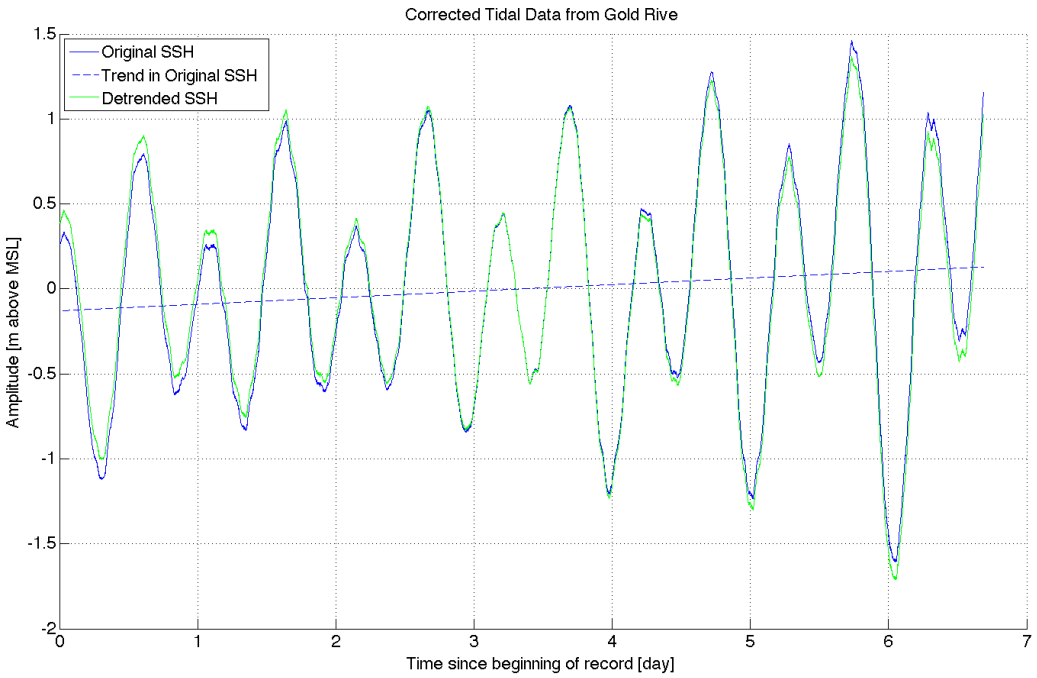

Figure 7: Raw observed Gold River tidal data in green, with linear trend in dashed blue. Detrended tidal data shown in solid blue.

Gold River Tidal Constituents

Constituent	Period [hr]	Amplitude [m]	Phase [radians]
M2	12.4206	0.9082	0.7190]
S2	12	0.2415	-1.9765
N2	12.6583	0.0548	-2.7135
K1	23.9344	0.2625	2.1444
O1	25.8193	0.2434	0.0430

Table 2: Major five tidal constituents present at the validation Gold River station

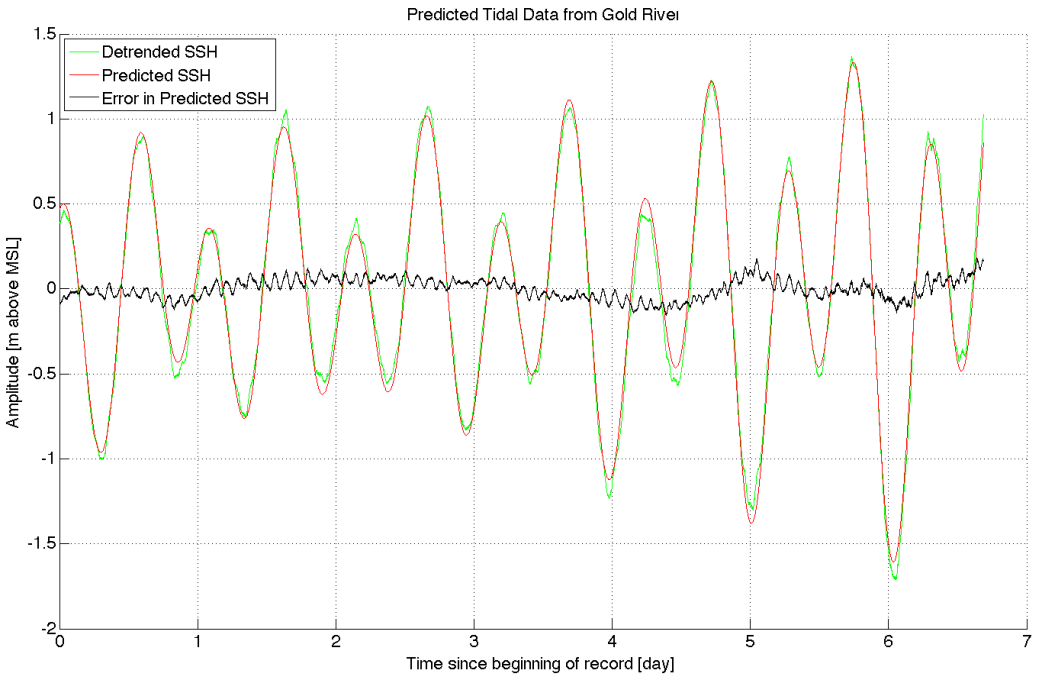

Figure 8: The predicted Gold River tide in red compared to the observed data minus the linear trend in green. The difference between the two is shown in black.

3.3. Validation

Validation of model results was performed by calculating both the Mean Absolute Error and Root Mean Square Error between the simulated and observed sea surface height at both the forcing Gore Island station and the validation Gold River station with 0m of sea level rise.

	MAE	RMSE
Gore Island	0.0624	0.0744
Gold River	0.0560	0.0687

Table 3: Validation results, showing the error between the simulated and observed sea surface height at two locations in the model.

3.4. Kinetic Energy

Figure 9 shows the mean amount of kinetic energy present throughout the model domain, with sea levels at the present level and 2 m higher than current levels. Note that these runs are the time-average of two separate 10 day simulations.

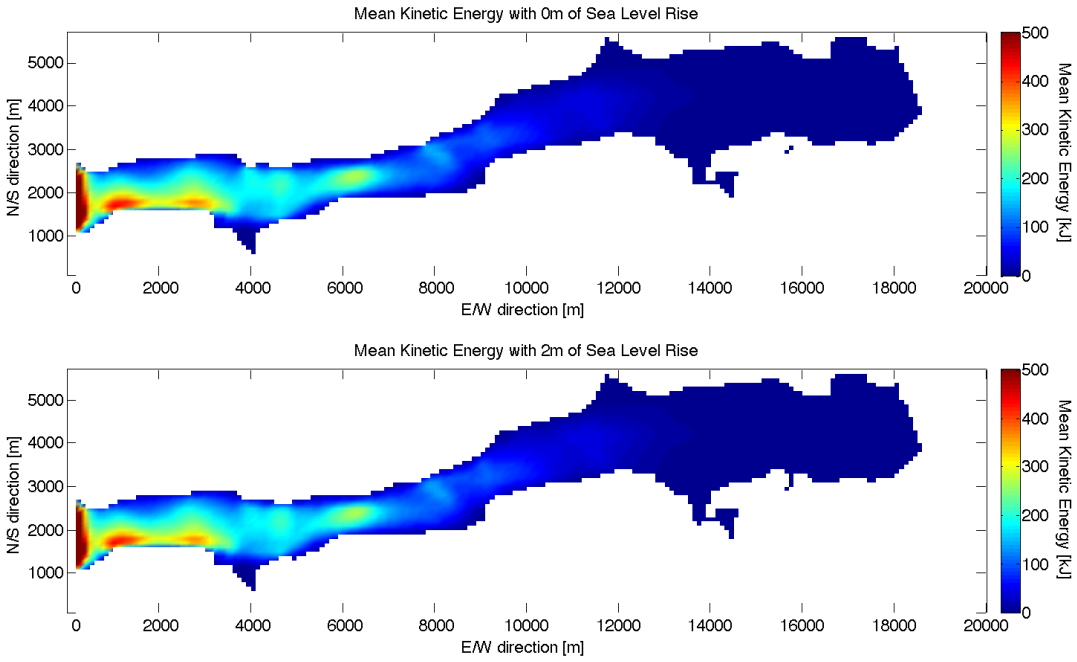

Figure 9: The temporally-meaned kinetic energy present throughout the model domain. The top figure shows a simulation with 0m of sea level rise, while the bottom figure shows a simulation with 2m of sea level rise. Note that the runs appear almost identical in this figure. The differences are highlighted in Figure 10

Kinetic energy seems to be concentrated near the boundary, at the westernmost sill, and at the shoreline. It also seems to greatly disperse as it moves further into the fjord, until it goes to almost zero at the fjord head.

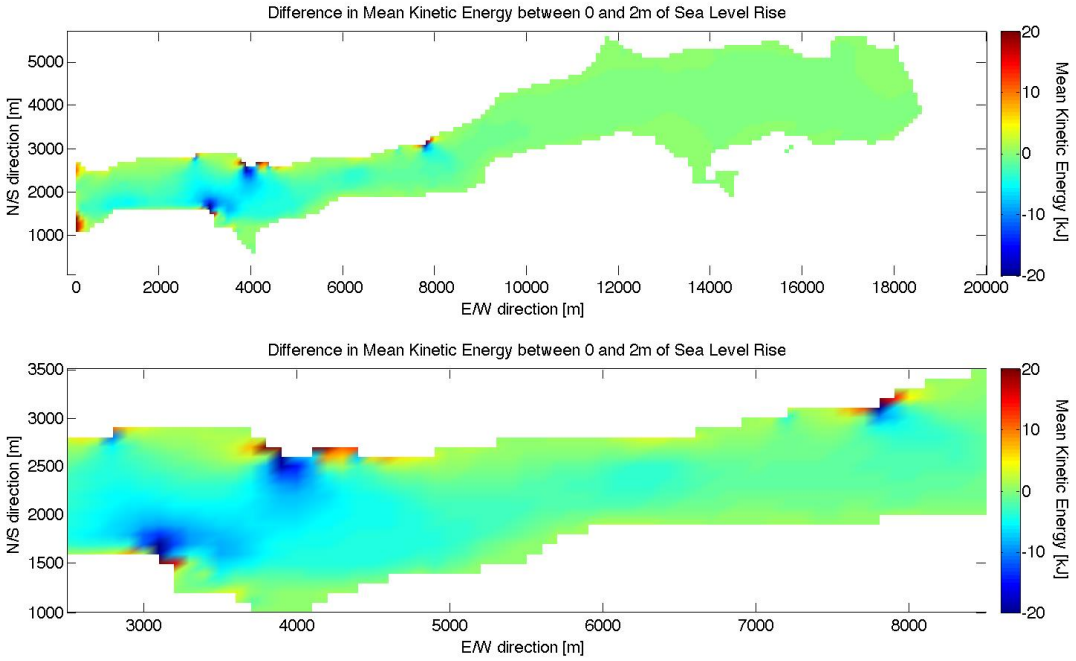

Figure 10: The difference in mean kinetic energy throughout the model domain, with the bottom figure being an enlarged version of the most active part of the top figure. Note that the color axis is one order of magnitude smaller in this figure than in Figure 9.

The difference in mean kinetic energy is also mostly present near the mouth of the inlet at the sill. Interestingly enough, there are adjacent locations that see increased and decreased kinetic energy, on the order of +/- 10%.

4. Discussion

4.1. Bathymetry

The bathymetry of the area had a few notable features. First and foremost a sill is evident between 2500 and 5000 m along the fjord. Secondly a number of submarine deltas can be observed along the channel of the fjord. These features are significantly shallower than the rest of the fjord, and thus alter the flow of water in the fjord in interesting ways. Finally, a large body of water is absent on the west side of the fjord. In reality, this body is connected to the

main channel, but in the data set I acquired no such body existed. This undoubtedly influenced my results, although despite the absence of this channel the model produced valid results (Table 3 and section 4.3).

4.2. Tides

A significant linear trend was present in both tidal datasets. This trend resulted in an increase of approximately 0.4 m at Gore Island and 0.3 m at Gold River over the course of the week. This is likely due to wind setup, which could be determined through examination of local weather patterns at the time that the measurements were taken. A higher frequency oscillation can also be observed in the tidal record, which is likely the result of a seiche moving up and down the channel.

4.3. Validation

The MAE and RMSE of the forcing data at the Gore Island station serve as our baseline for comparison when determining whether or not the model is valid, which we compare to the MAE and RMSE of the validation data at the Gold River station. Both the MAE and the RMSE were less at the validation Gold River station than at the forcing Gore Island station, but not overwhelmingly so. This shows that the forcing data induces the correct response in the validation data, which indicates that the model is producing accurate, realistic results. Thus we are able to draw meaningful conclusions from data produced by the model.

4.4. Kinetic Energy

The distribution of kinetic energy throughout the model was surprisingly similar in both cases. Differences were largest at headlands near the fjord mouth and at the sill. These

differences were on the order of +/- 10%, which is a significant fraction of the overall kinetic energy at those locations. Furthermore, increases and decreases occurred adjacent to one another, indicating that kinetic energy is moving away from the center of the sill to the sides of headlands near the sill. This movement of kinetic energy means that the center of the channel should experience less flow energy while the edges should experience more. This may have significant impacts, namely as an increase in erosion in these side-headland areas due to the increase in energetic flow at these sites and an increase in deposition at the head of the headland areas due to the decrease in energetic flow there. While there may also be some effects on the biological communities from the movement of energy, due to the highly localized nature of the change in energy the impact on biology is expected to be less significant than that on erosive shoreline processes. This change in erosion and deposition could also alter the nearshore and intertidal environments, which could impact the biology that lives there. Given time, this could additionally result in significant reshaping of these headlands and an overall restructuring of the fjord mouth, which could further impact circulation in the area. Further investigation could yield valuable insight into precisely how erosion and deposition could be expected to change given future sea level rise, and what the specific effects will be in places like Muchalat Inlet.

4.5. Limitations

Major limiting factors include the idealization of oceanic conditions and tidal circulation, in addition to limits imposed by the data. The model assumes that the only forces acting on water parcels are the pressure gradient force calculated from the shallow-water equations [1-5] and frictional forces calculated form the quadratic bottom friction equation [6, 7]. This means

that the effects of wind-generated surface waves and wind stress on the sea surface were ignored. This idealization proved to be useful, as the study is primarily interested in tidal circulation so omitting these additional forces helped to increase clarity in the investigation. As the model was two-dimensional and not fully three-dimensional, it assumed homogeneity in the water column and was therefore be unable to simulate the stratified flow typically seen in estuaries. Despite this limitation, the model still accurately simulated tidal circulation at a high level (Table 3 and section 4.3).

The primary limiting factors in the various datasets were due to the length of the tidal record, the quality of the bathymetric data, and the available computation time. Tide gauges were only deployed for approximately one week, which meant that only the larger tidal constituents could be accurately resolved. While these larger constituents do account for the majority of the observed tides, a longer record could give more accurate forcing data, which could in turn improve the model accuracy. The bathymetric data was low-resolution and in some areas wildly inaccurate. While the model still produced accurate predictions with this rather idealized bathymetric representation, a more true-to-life data set could yield more interesting results. Finally, simulations took a significant amount of time to compute. Given more time, month-long simulations could be performed which may change results slightly, although the general conclusions would likely remain the same. Despite these data limitations, the model managed to provide accurate results.

5. Conclusions

Kinetic energy in the fjord was generally concentrated at the mouth of the inlet, specifically over and around the sill. With sea level rise a decrease in kinetic energy was observed above the middle of the sill while an increase in kinetic energy was observe toward the sides of the sill. This indicates that sea level rise will cause significant changes to the circulation patterns of the fjord, and may alter processes like the erosion and deposition of sediment at the mouth of the fjord. Further investigations spanning longer time series should reveal more details regarding the specific impacts of sea level rise in fjords, but this study serves to indicate some of the possible impacts that may occur.

6. References

Arakawa, A., V. Lamb. 1977. Computational design of the basic dynamical processes of the UCLA general circulation model. Methods of Comp. Phys. **17**: 173–265.

Calder, B. and L. Mayer. 2001. Automatic processing of high-rate, high-density multibeam echosounder data. Geochem. Geophys. Geosys. **4**: 1-22.

Church, J., P. Clark, A. Cazenave, J. Gregory, S. Jevrejeva, A. Levermann, M. Merrifield, G. Milne, R., Nerem, P. Nunn, A. Payne, W. Pfeffer, D. Stammer and A. Unnikrishnan. 2013. Sea Level Change. *In* T. Stocker, D. Qin, G. Plattner, M. Tignor, S. Allen, J. Boschung, A. Nauels, Y. Xia, V. Bex and P. Midgley [eds.], Climate Change 2013: The Physical Science Basis. Contribution of Working Group I to the Fifth Assessment Report of the Intergovernmental Panel on Climate Change. Cambridge University Press, Cambridge, United Kingdom and New York, NY, USA.

Crean, P.B., 1978. A numerical model of barotropic mixed tides between Vancouver Island and the mainland and its relation to studies of the estuarine circulation. Hydrodynamics of Estuaries and Fjords. **23**: 283-313.

Durran, D. 1998. Numerical methods for fluid dynamics: with application in geophysics. 1st ed. Springer.

Holleman, R. and M. Stacey. 2014. Coupling of sea level rise, tidal amplification, and inundation. Jo. of Phys. Ocean. **44**: 1439-1455.

Kawase, M. and B. Bang. 2013. Seasonal variability of salinity and circulation in a silled estuarine fjord: A numerical model study.Cont. Shelf Res. **71**: 131-152.

Pelling, H. and J. Mattias Green. 2014. Impact of flood defences and sea-level rise on the European Shelf tidal regime. Cont. Shelf Res. **85**: 96-105.

Salehipour, H., G. Stuhne, and W. Peltier. 2013. A higher order discontinuous Galerkin global shallow water model: Global ocean tides and aquaplanet benchmarks. Ocean Modelling. **69**: 93-107.

Schureman, Paul. 1958. Manual of harmonic analysis and prediction of tides. U.S. Government Printing Office, Washington D.C.

Shugar, D., I. Walker, O. Lian, J. Eamer, C. Neudorf, D. McLaren, and D. Fedje. 2014. Post-glacial sea-level change along the Pacific coast of North America. Quarter. Sci. Rev. **97**: 170-192.